PNAS RESEARCH ARTICLE | NEUROSCIENCE

Mitochondrial control of microglial phagocytosis by the translocator protein and hexokinase 2 in Alzheimer's disease

Lauren H. Fairley[a,1], Kei Onn Lai[a,1], Jia Hui Wong[a,1], Wei Jing Chong[a], Anselm Salvatore Vincent[a], Giuseppe D'Agostino[b], Xiaoting Wu[c], Roshan R. Naik[a], Anusha Jayaraman[d], Sarah R. Langley[b], Christiane Ruedl[c], and Anna M. Barron[a,2]

Edited by Patrick Stover, Texas A&M AgriLife, College Station, TX; received May 30, 2022; accepted December 17, 2022

Microglial phagocytosis is an energetically demanding process that plays a critical role in the removal of toxic protein aggregates in Alzheimer's disease (AD). Recent evidence indicates that a switch in energy production from mitochondrial respiration to glycolysis disrupts this important protective microglial function and may provide therapeutic targets for AD. Here, we demonstrate that the translocator protein (TSPO) and a member of its mitochondrial complex, hexokinase-2 (HK), play critical roles in microglial respiratory-glycolytic metabolism and phagocytosis. Pharmacological and genetic loss-of-function experiments showed that TSPO is critical for microglial respiratory metabolism and energy supply for phagocytosis, and its expression is enriched in phagocytic microglia of AD mice. Meanwhile, HK controlled glycolytic metabolism and phagocytosis via mitochondrial binding or displacement. In cultured microglia, TSPO deletion impaired mitochondrial respiration and increased mitochondrial recruitment of HK, inducing a switch to glycolysis and reducing phagocytosis. To determine the functional significance of mitochondrial HK recruitment, we developed an optogenetic tool for reversible control of HK localization. Displacement of mitochondrial HK inhibited glycolysis and improved phagocytosis in TSPO-knockout microglia. Mitochondrial HK recruitment also coordinated the inflammatory switch to glycolysis that occurs in response to lipopolysaccharide in normal microglia. Interestingly, cytosolic HK increased phagocytosis independent of its metabolic activity, indicating an immune signaling function. Alzheimer's beta amyloid drastically stimulated mitochondrial HK recruitment in cultured microglia, which may contribute to microglial dysfunction in AD. Thus, targeting mitochondrial HK may offer an immunotherapeutic approach to promote phagocytic microglial function in AD.

immunometabolism | mitochondria | hexokinase | translocator protein | Alzheimer's disease

Mitochondria are emerging as the command centers of innate immune responses, controlling inflammatory responses via metabolic programming; this is known as immuno-metabolism (reviewed in ref. 1). Recent evidence indicates that in Alzheimer's disease (AD), metabolic programming breaks down in microglia, which are the resident innate immune cells of the brain, thereby disrupting important protective functions of these cells such as phagocytosis (2). Microglial phagocytosis plays a key role in the clearance of toxic beta amyloid (Aβ), aggregations of which are a hallmark of AD (3). The mechanisms coordinating mitochondrial metabolism to fuel phagocytosis, which are disrupted in AD, remain poorly understood. Here, we investigate the role of the mitochondrial translocator protein (TSPO) complex in microglial metabolic programming and phagocytosis in AD-related inflammation.

TSPO is a positron emission tomography (PET)-visible inflammatory biomarker (reviewed in ref. 4) and therapeutic target in AD (5–7). Microglial TSPO expression is upregulated in AD, correlating with the distribution of pathological aggregates of Aβ and tauopathy (8, 9). However, despite being widely regarded as a marker of microglial activation, the specific immunophenotype associated with TSPO and whether TSPO modulates beneficial or detrimental microglial functions in AD have not been determined. Further, the function of TSPO in microglial immune responses and AD pathogenesis remains unclear. In mouse models of AD, we and others have shown that TSPO-targeting drugs reduce Aβ accumulation and neuronal death (5, 7, 10). While TSPO has been implicated in a range of microglial inflammatory responses, including cytokine secretion, proliferation, motility, and phagocytosis (11–13), the mechanisms underlying the protective effects of TSPO-targeted drugs in AD are not understood.

One possibility is that TSPO regulates microglial inflammatory responses via metabolic reprogramming (14–17). Proinflammatory activation of microglia is dependent upon a switch in energy production through mitochondrial respiration via oxidative phosphorylation (OXPHOS) to glycolysis (18–22). Increased glycolysis is associated with aging

Significance

Microglia are responsible for protecting the brain. Defense demands the rapid production of large amounts of energy. But how microglial metabolism is controlled to fuel defense responses such as phagocytosis remains poorly understood. We demonstrate that mitochondrial translocator protein (TSPO) and hexokinase-2 play key roles in the control of microglial metabolism and phagocytosis by coordinating the balance of energy production via two major metabolic pathways. Microglia lacking TSPO resembled dysfunctional microglia observed in aging and Alzheimer's disease, and this could be partially reversed by blocking hexokinase-2 binding to the mitochondria. We find that targeting mitochondrial hexokinase-2 binding may offer an immunotherapeutic approach to inhibit glycolytic metabolic reprogramming and promote microglial phagocytosis in Alzheimer's disease.

Preprint: https://www.biorxiv.org/content/10.1101/2021.12.01.469111v1.full.

Author contributions: L.H.F., K.O.L., J.H.W., and A.M.B. designed research; L.H.F., K.O.L., J.H.W., W.J.C., A.S.V., X.W., R.R.N., A.J., and A.M.B. performed research; L.H.F., K.O.L., J.H.W., W.J.C., G.D., S.R.L., C.R., and A.M.B. analyzed data; and L.H.F., K.O.L., J.H.W., and A.M.B. wrote the paper.

The authors declare no competing interest.

This article is a PNAS Direct Submission.

[1]L.H.F., K.O.L., and J.H.W. contributed equally to this work.

[2]To whom correspondence may be addressed. Email: barron@ntu.edu.sg.

This article contains supporting information online at https://www.pnas.org/lookup/suppl/doi:10.1073/pnas.2209177120/-/DCSupplemental.

Published February 14, 2023.

and AD, linked to compromised phagocytosis and Aβ engulfment (reviewed in ref. 1). This switch to aerobic glycolysis is known as the Warburg effect, originally described in cancer. In cancer, the balance of oxidative and nonoxidative glucose metabolism is coordinated by the voltage-dependent anion channel (VDAC), which forms part of a mitochondrial complex with TSPO (23–25).

VDAC is a mitochondrial hub protein and the major channel for supply of mitochondrial substrates to fuel OXPHOS. In other cell types, binding of VDAC to the glycolytic enzyme hexokinase-2 (HK) allosterically increases its activity to promote glycolysis whilst inhibiting OXPHOS (26). Although there is currently little agreement on what interactors form the functional complex with TSPO in the neuroimmunological context, the same HK isoform is expressed by microglia and is known to play a critical role in mediating inflammatory activation (27).

To determine the TSPO-associated immunological signature in a model of neuroinflammation, we examined the effect of TSPO deletion (TSPO-KO) on microglial function in models of AD-related inflammation. We found that TSPO plays a critical role in microglial energy production via OXPHOS to fuel phagocytosis. Further, we discovered new evidence that microglial metabolic programming and phagocytic function is regulated through changes in subcellular localization of the key metabolic enzyme, HK. Based on these findings, we propose that mitochondrial TSPO and HK are a critical hub regulating the glycolytic-respiratory metabolic balance and phagocytosis in microglia.

Results

TSPO Deletion Alters Transcriptional Profiles in Phagocytosis, Mitochondrial Metabolism, and Lipid Biosynthesis in Neuroinflammation. To determine the effect of TSPO deletion on neuroinflammatory responses, lipopolysaccharide (LPS)-induced transcriptional profiles in the hippocampus of wildtype (WT) and global TSPO-KO mice were compared by RNAseq. Under control conditions, little effect of TSPO-KO was observed on transcription, with only 27 significantly differentially expressed genes (DEGs, false discovery rate (FDR) < 0.05, $\log_2$ (fold change) ≥ 0.5 or ≤ −0.5; Fig. 1*A*). This was too few DEGs to investigate further using over-representation or enrichment analyses. In contrast, following stimulation with LPS, robust transcriptional differences were observed between TSPO-KO and WT mice, with 795 significantly DEGs, supporting the notion that TSPO plays a role in inflammatory responses in the brain (545 downregulated, 250 upregulated; Fig. 1*A* and *SI Appendix*, Table S2). Fast gene set enrichment analysis (fGSEA) comparing LPS-stimulated TSPO-KO and WT mice showed downregulation of immune and inflammatory pathways and upregulation of mitochondrial and lipid metabolism pathways (Fig. 1*B* and *SI Appendix*, Table S3).

Top downregulated immune-related processes were phagocytosis and responses to tumor necrosis factor (TNF) and interferon (IFN) signaling. Downregulation of phagocytosis-related pathways included genes involved in phagocytic cup formation and closure (*Inpp5b, Irgm1,* and *Dnm2*), phagosome acidification and respiratory burst (*Slc11a1*, *Atp6v0e, Cyb,* and *Ncf1,2,4*), phagosolysosome assembly and maturation (*Coro1a, Rab, Rac,* and *Vav*), and expression of phagocytosis receptors (*Fcγr-Fcgr, Bin2, Cr1l, Cr3, Itgam, Itgb2, Tlr1, Tlr2, Cd14, Msr1,* and *Marco*) (Fig. 1 *B* and *C*). Key genes in downregulated TNF and IFN signaling pathways in TSPO-KO mice included *Tnf*, *Tnfsf*-10, and *Tnfrsf* (13b,14). Genes involved in antigen processing and presentation (*Tap, H2-M3,* and *H2-T23*) and complement cascade (*C3, C5,* and *Cf b*) were also downregulated. These findings support a key role for TSPO in neuroinflammatory responses, particularly phagocytosis and cytokine signaling.

Supporting existing consensus on TSPO's role as a mitochondrial metabolic target, upregulation of genes encoding subunits of mitochondrial complexes I, II, and IV was observed (*Nd, Ndufa-c, Ndufs, Sdh,* and *Cox*). Likewise, cholesterol and fatty acid biosynthesis genes were upregulated (*Acsl, Acsbg1, Ch25h, Fasn, Elovl,* and *Mvd*), while synthesis and metabolism of the inflammatory eicanosinoids were downregulated (*Aloxe3, Alox5, Alox5ap,* and *Ptges*) in LPS-stimulated TSPO-KO mice (Fig. 1 *B* and *C*). Other functionally enriched pathways included downregulation of transcription and translational responses, apoptosis and cell-death–related pathways, and upregulation of terms related to nervous system development, myelination, ion homeostasis, and excitatory/inhibitory neurotransmission, including gamma-aminobutyric acid (GABA)-ergic neurotransmission-related pathways.

Proteomic TSPO Interactome Network in AD. To gain insight into the protein–protein interactions and molecular pathways underlying TSPO complex function in the brain, the TSPO interactome was captured by co-IP-MS under control and AD inflammatory conditions using WT and APP-KI mouse brain. A total of 124 proteins were identified as candidate TSPO interactors, significantly enriched relative to TSPO-KO background (*SI Appendix*, Table S4).

Analysis of the candidate TSPO interactors for known physical protein–protein interactions using IntAct database revealed that the 14-3-3 family scaffold adaptor and chaperone proteins, Ywhae, Ywhag, and Ywhaz, interact with the majority of the identified TSPO interactors (87.5%, 63.3%, and 48.3% of TSPO interactors, respectively; FDR < 0.0001). This identified the 14-3-3 adaptor proteins as a hub in the brain TSPO interactome. The brain TSPO interactome network was mapped using STRING network analysis (Fig. 1 *D*–*F*). Of the 124 identified candidate interactors, 44 were enriched from the mitochondrial compartment. Functional enrichment of metabolism pathways and immune system was observed in the TSPO interactome network (FDR < 0.05; Fig. 1*F* and *SI Appendix*, Table S5). Metabolism pathways included the pentose phosphate pathway, gluconeogenesis/glycolysis, tricarboxylic acid (TCA) cycle, OXPHOS, and fatty acid metabolism. Immune system functions included phagosome-related networks, including vacuolar ATPase involved in phagosome acidification and cytoskeletal elements involved in phagosome transport. The vacuolar ATPase node involved in phagosome acidification contained proteins that have previously been identified as microglial enriched relative to other brain cells (Atp6v1a, Atp6v1b2, Atp6v0a1, and Atp6v1c1) (28). Functional enrichment of terms relating to neurotransmission (including GABA synthesis, release, reuptake, and degradation) and neurodegenerative disease (including AD, Parkinson disease, Prion disease, Huntington disease, and Amyotrophic lateral sclerosis) was also observed.

TSPO-KO Induces Mitochondrial HK (mtHK) Binding and a Switch to Nonoxidative Cellular Bioenergetics in Cultured Microglia. Since our transcriptomic and proteomic data implicated TSPO in metabolism pathways and immune function, and immunohistochemical analysis of wild type (WT) and amyloid precursor protein knock-in (APP-KI) mouse brain showed TSPO is predominantly expressed by microglia (*SI Appendix*, Fig. S1), we examined the effect of TSPO-KO on cellular bioenergetics in primary cultured mouse microglia. TSPO-KO microglia exhibited impaired mitochondrial OXPHOS and reduced mitochondrial ATP levels (Fig. 2 *A*–*C*). A marked reduction in basal respiration (*t* test: CI = −77.6, −60.3; $P < 0.0001$), maximal respiration (*t* test: CI = −1.05e+02, −48.2; $P = 0.0014$) and ATP production (*t* test: CI = –

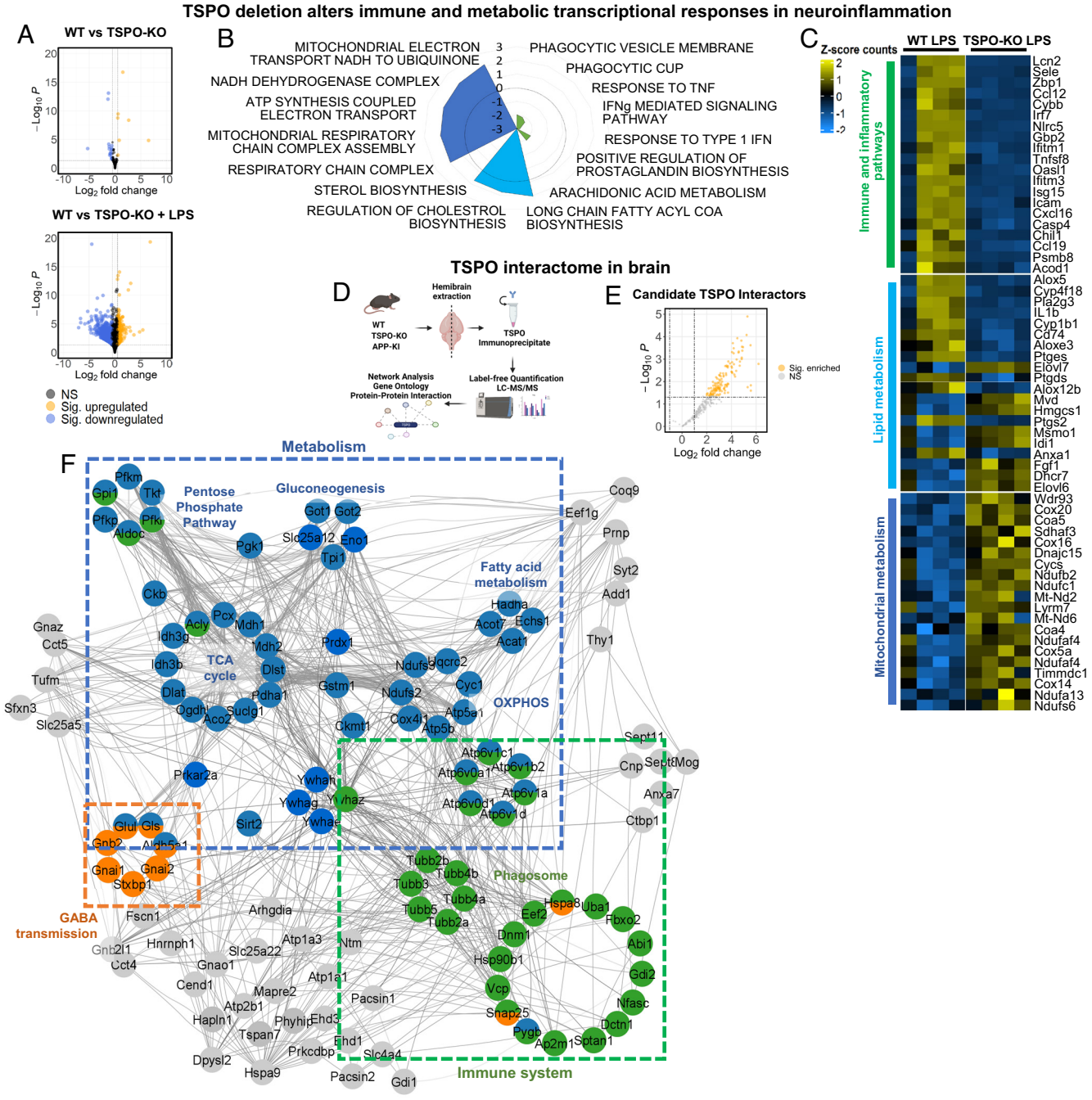

Fig. 1. TSPO function associated with mitochondrial bioenergetics, lipid metabolism and phagocytosis pathways in mouse models of AD-related neuroinflammation. (*A*) Volcano plot showing DEGs in hippocampus of WT vs. TSPO-KO mice (n = 4 mice/group). (*B*) Normalized enrichment score of top enriched Gene Ontology pathways related to immune and inflammatory responses, mitochondrial and lipid metabolism identified by fGSEA analysis of LPS treated WT vs. TSPO-KO mice. (*C*) Heat map of mean gene expression for selected enriched immune, mitochondrial and lipid metabolism pathways in LPS treated WT and TSPO-KO mice. (*D*) Schematic of proteomic TSPO interactome analysis in brain. TSPO complexes were isolated via immunoprecipitation from wildtype and APP-KI mouse brains, using TSPO-KO as a background control. Enriched proteins were identified by liquid chromatography-tandem mass spectrometry (LC-MS/MS) and the interactome network mapped using bioinformatics approaches. Created with BioRender.com. (*E*) Volcano plot showing proteins identified by TSPO IP-MS, with candidate TSPO interactors (orange data points) identified as greater than twofold significantly enriched compared to background (TSPO-KO). (*F*) Brain TSPO interactome protein-protein interaction network showing significantly enriched functional clusters in immune system and metabolic pathways. *A*, *B*, and *F*: Benjamini Hochberg (BH) corrected FDR <0.05; NS, non-significant. E: Limma differential enrichment analysis, BH corrected FDR <0.1.

53.0, −42.2; $P < 0.0001$) as measured by oxygen consumption rate (OCR) in the Seahorse Mito Stress test was observed in TSPO-KO microglial cultures (Fig. 2*B*). Reduced mitochondrial ATP signals in TSPO-KO microglia was confirmed using the live-cell imaging switchable fluorescent ATP probe, ATP-Red (Fig. 2*C*). Reduced mitochondrial membrane potential as measured by tetramethylrhodamine, ethyl ester (TMRE) fluorescence was also observed in TSPO-KO microglia (*t* test: CI = −0.795, −0.508, $P = 0.0034$; n = 4 to 6 wells), consistent with respiratory chain defects and reduced OXPHOS (*SI Appendix*, Fig. S2*A*). A modest reduction in mitochondrial content as measured by footprint and increase in mitochondrial fragmentation was also observed in TSPO-KO microglia under baseline conditions (mitochondrial footprint *t* test: CI = −7.47, −1.9; $P = 0.001$; fragmentation *t* test: CI = 0.0144 to 0.12, $P = 0.0196$; *SI Appendix*, Fig. S2 *B–D*). These findings suggest TSPO plays a critical role in

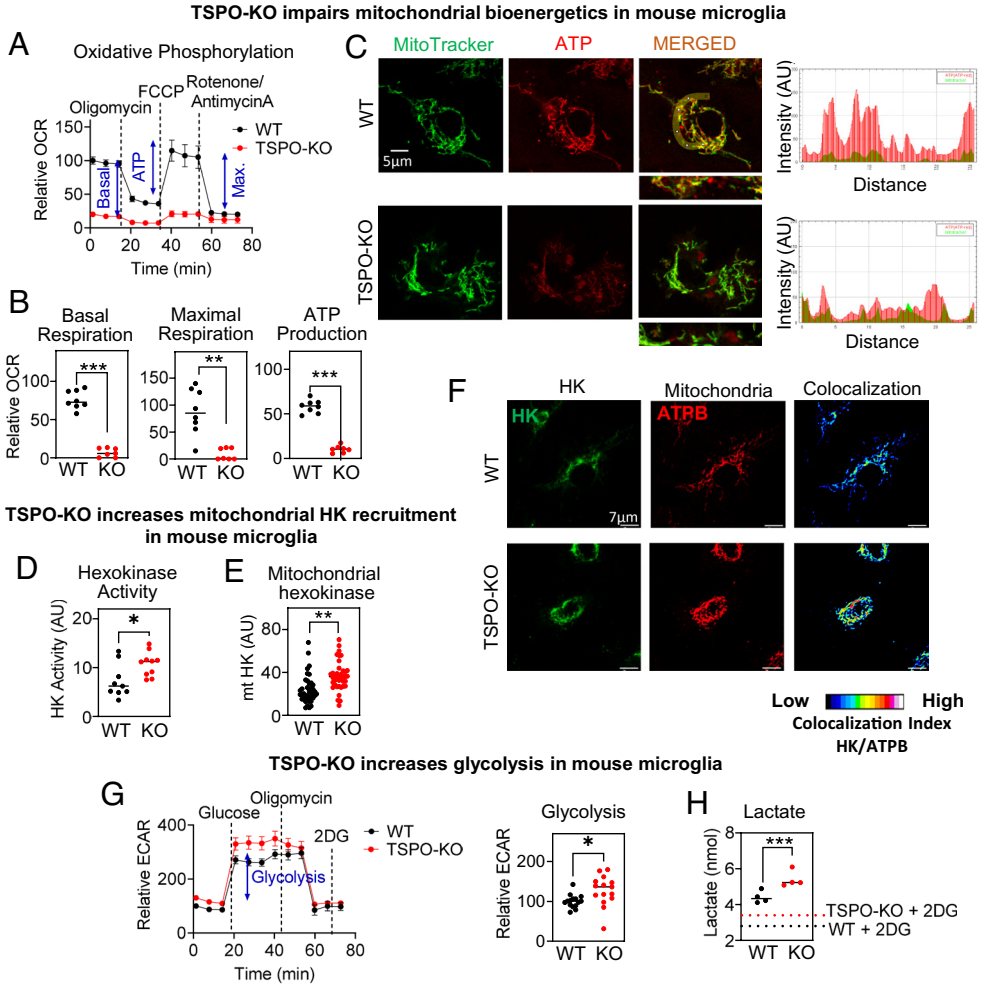

Fig. 2. TSPO deletion induces mtHK binding and impairs mitochondrial bioenergetics in mouse microglia. (*A*) Seahorse Mitostress test of WT and TSPO-KO cultured primary mouse microglia showing mean ± SEM OCR normalized to WT. Basal respiration (basal), ATP production (ATP) and maximal respiration (max.) indicated on WT curve. ATP synthase inhibitor, oligomycin was injected to inhibit ATP-linked mitochondrial respiration as a measure of mitochondrial ATP production. To determine maximal respiration, the mitochondrial uncoupler carbonyl cyanide p-(trifluoromethoxy) phenylhydrazone (FCCP) was injected. To determine the contribution of non-mitochondrial respiration to the OCR, a mixture of rotenone and antimycin was injected, inhibiting mitochondrial respiration. (n = 7 to 8 wells/group, average of two independent experiments). (*B*) Quantification of basal respiration, maximal respiration, and ATP production calculated from Mitostress assay. Dots represent individual wells. (*C*) Representative image of MitoTracker (green) and intracellular ATP signals (red) in cultured WT and TSPO-KO primary mouse microglia. Reduced ATP signals in the mitochondrial compartment evident in the merged panel (colocalization indicated in yellow). Histogram indicates ATP-Red 1 and MitoTracker intensity in line indicated on merged image. (*D*) HK activity measured in primary mouse microglia cell lysates. Dots represent individual wells (n = 9 to 10/group, average of two independent experiments). (*E*) mtHK binding measured by mean HK immunoreactive intensity within mitochondrial volumes determined using ATP synthase subunit beta (ATPB) staining in WT and TSPO-KO mouse microglial cultures. Dots represent individual cells (n = 40/group, average of two independent experiments). (*F*) Representative confocal images of HK immunoreactivity (*Left*, HK, green), mitochondria (*Middle*, ATPB, red), and colocalization index of HK relative to ATPB immunoreactivity (*Right*). AU: arbitrary units. (*G*) Glycolysis test curve (*Left*, mean ± SEM) and quantification of glycolytic rate (*Right*) in cultured WT and TSPO-KO primary mouse microglia. Data shown as mean ± SEM ECAR normalized to WT. Glucose was injected as a substrate for glycolysis. ATP synthase inhibitor, oligomycin was injected to stimulate maximal dependence on glycolysis. 2DG was injected to competitively inhibit glucose uptake to determine non-glycolytic ECAR. (n = 15 wells/group, average of two independent experiments). (*H*) Lactate concentrations measured in culture media of WT and TSPO-KO primary mouse microglia. Dots represent individual wells. (n = 4/group). WT vs. TSPO-KO groups in all figures analyzed by unpaired two-sided permutation *t* test. **P* < 0.05. ***P* < 0.002. ****P* < 0.0001.

microglial ATP production via OXPHOS. Supporting this, the TSPO agonist Ro5-4864 increased OXPHOS in immortalized microglial BV2 cells as measured by OCR in the Seahorse Mito Stress (*SI Appendix*, Fig. S3*A*).

Mitochondrial metabolic impairment in TSPO-KO microglia was coupled with elevated activity of the rate-limiting glucose metabolizing enzyme, HK (*t* test: CI = 0.63, 5.76, *P* = 0.0252; n = 9 to 10 wells/group, average of two independent experiments; Fig. 2*D*). In other cell types, HK has been shown to bind to the TSPO complex member, VDAC, where rβecruitment of HK from the cytosol to the mitochondria allosterically increases its enzymatic activity (29). Consistent with this, increased mtHK binding was observed in TSPO-KO microglia, suggesting that loss of TSPO activity increases mitochondrial HK recruitment (*t* test: CI = 6.97 to 18.5, *P* = 0.0002; n = 40 individual cells/group, average of two independent experiments; Fig. 2 *E* and *F*). This was coupled with a modest increase in glycolysis in cultured TSPO-KO microglia measured by extracellular acidification rate (ECAR) in the Seahorse Glycostress test (*t* test: CI = 4.26, 44.4; *P* = 0.014; n = 15 wells, average of two experiments; Fig. 2*G*). Elevated levels of the glycolytic metabolite, lactate, were also observed in the media of TSPO-KO microglial cultures (*t* test: CI = 0.583, 1.54; *P* < 0.0001; n = 4 wells/group; Fig. 2*H*). Interestingly, this increase in mtHK binding was observed in TSPO-KO microglia despite a modest but significant decrease in HK messenger RNA (mRNA) expression in the mouse brain following LPS stimulation (log2 (fold change): −0.548, *P* = 0.013). Increased glycolysis in TSPO-KO microglia may be a compensatory response to the severe OXPHOS deficits resulting from loss of TSPO function since the TSPO agonist Ro5-4864 did not alter glycolysis in immortalized microglial BV2 cells (*SI Appendix*, Fig. S3*B*).

TSPO Deletion Induces Microglial Lipid Droplet Accumulation. Since metabolic reprogramming from OXPHOS to glycolysis is associated with lipid droplet formation in aging and disease (30), we investigated lipid droplet accumulation in primary microglial cultures using the neutral lipid marker, 4,4-difluoro-4-bora-3a, 4a-diaza-s-indacene (BODIPY)–FLC12 (BD). Consistent with the transcriptomic and proteomic data suggesting a role for TSPO in fatty acid synthesis and metabolism, primary microglia isolated from TSPO-KO mice exhibited enhanced lipid droplet accumulation compared to WT primary microglia (two-way ANOVA; Main Effect (Genotype): $F_{(1, 30)} = 45.668$; $P < 0.001$), and LPS markedly exacerbated lipid droplet accumulation in both cultured TSPO-KO and WT microglia (two-way ANOVA; Main Effect (Treatment): $F_{(1, 30)} = 23.018$; $P < 0.001$; n = 9/group, average of three independent experiments, Fig. 3 *A* and

B). In contrast, TSPO agonist, Ro5-4864, reduced LPS-induced lipid droplet accumulation in immortalized microglial BV2 cells (two-way ANOVA; Interaction Effect (Treatment × LPS): $F_{(1, 32)} = 52.668$; $P < 0.001$; Bonferroni-corrected pairwise comparison, LPS condition Vehicle vs. Ro5-4864: $P < 0.0001$; n = 9/group, average of three independent experiments; Fig. 3*C*). In the mouse brain, significantly lower TSPO expression was observed in the LPS-induced lipid droplet accumulating microglial subpopulation (*t* test: *CI* = −7.78, −2.19, $P < 0.001$; n = 3 mice; *SI Appendix*, Fig. S4*A*). A recent study has associated lipid droplet accumulation with phagocytosis-impaired, dysfunctional microglial phenotypes that develop in aging (31). Consistent with this, we observed reduced levels of the lipid droplet marker, perilipin 2, in phagocytic compared to nonphagocytic primary WT microglia (*t* test: CI = −7.07e+03, −2.93e+03; $P < 0.0001$; n = 3/group; *SI Appendix*, Fig S4*B*).

TSPO Modulates Aβ Phagocytosis in Cultured Microglia. Next, we investigated the effect of TSPO-KO on phagocytic functions in microglia, which play an important protective function in AD through clearance of Aβ. Cultured mouse TSPO-KO microglia exhibited impaired phagocytosis of Aβ compared to WT microglia measured by flow cytometry (*t* test: CI = −67.5, −53.6; $P = <0.0001$; n = 9/group, average of three experiments; Fig. 3*D*) and visually confirmed by immunocytochemistry (Fig. 3*E*). Conversely, treatment with the TSPO agonist, Ro5-4864, increased phagocytosis of Aβ in immortalized microglial BV2 cells measured by flow cytometry (*t* test: CI = 3.26, 31.9; $P = 0.0442$; n = 12/group, average of four experiments; Fig. 3*F*) and confirmed by immunocytochemistry (Fig. 3*G* and *SI Appendix*, Fig. S5*A*). The specificity of Ro5-4864 action for TSPO was verified in TSPO-KO microglia, with no effect of Ro5-4864 on Aβ phagocytosis observed in TSPO-KO microglia (*t* test: CI = −4.07, 0.975, $P = 0.23$, n = 4 to 5 wells/group; *SI Appendix*, Fig. S5*B*). To test the contribution of cell membrane-bound Aβ to signals measured by flow cytometry, cells were incubated at 4 °C, which inhibits phagocytic activity. Negligible Aβ levels were detected in Ro5-4864–treated cells incubated at 4 °C (Fig. 3*F*).

We hypothesized that metabolic deficiency in the TSPO-KO microglia would result in insufficient ATP production to support energy-demanding functions such as actin polymerization required for phagocytosis. Consistent with this hypothesis, TSPO-KO microglia exhibited a marked reduction in actin levels measured using the F-actin stain, phalloidin (*t* test: CI = −21.9, −9.39, $P < 0.0001$; n = 35 to 52 individual cells/group; *SI Appendix*, Fig. S6). TSPO-KO did not affect cell viability in LPS or Aβ-treated cultures (<1% propidium iodide$^+$ cells in vehicle, LPS, and Aβ treatment conditions measured via flow cytometry).

TSPO is Upregulated in Phagocytic Microglia, Surrounding Amyloid Plaques in Alzheimer's Brain. To investigate if the functional association between TSPO and phagocytosis is consistent with the phenotype of TSPO expression in AD, we investigated TSPO expression in actively phagocytosing myeloid cells isolated from the AD-mouse brain (APP-KI mice). Phagocytic cells were identified by the presence of internalized Aβ by flow cytometry (Fig. 4 *A*–*D*). The proportion of Aβ$^+$ phagocytes increased in APP-KI mice with age (one-way ANOVA; $F_{(2, 16)} = 118.3$ $P < 0.0001$; Bonferroni-corrected pairwise comparison (2 mo vs. 4 mo): $P = 0.08$, (4 mo vs. 9 mo): $P < 0.0001$; n = 6 to 7 mice/group; Fig. 4*A*), and the majority were identified as microglia through the expression of the microglia-specific marker TMEM199 (n = 5 APP-KI mice; Fig. 4*B*). Aβ$^+$ phagocytic microglia were characterized by elevated TSPO expression (Fig. 4*C*), as well as upregulated expression of MHCII, CD68, and CD11c, markers previously associated with activated, phagocytic microglia phenotypes in aging and AD (Fig. 4 *C* and *D*) (32). In contrast to Aβ$^-$ microglia, Aβ$^+$ microglia also exhibited high CD45 expression (Fig. 4 *D* and *E*), consistent with previous findings that CD45^{hi} populations are the most phagocytically active mononuclear phagocytes in the brain (33). Expression of the microglial marker purinergic receptor P2Y12 (P2RY12) further corroborated the microglial origin of the Aβ$^+$ phagocytes despite elevated CD45 expression. CD45, MHCII, and CD11c expression progressively increased in Aβ$^+$ phagocytic microglia as disease severity progressed in APP-KI mice between 5 and 10 mo of age, perhaps reflecting the functional specialization of these microglia in response to Aβ pathogenesis (Fig. 4*E*).

Since previous studies have implicated microglia clustered at Aβ plaques in phagocytic clearance (34), TSPO expression was analyzed by immunohistochemistry in mouse and human AD brains. Microglial TSPO immunoreactivity increased progressively between 4 and 9 mo of age (two-way ANOVA; Interaction (Genotype × Age): $F_{(1, 8)} = 6.625$, $P = 0.0329$; Bonferroni-corrected pairwise comparisons: (APP-KI 4 mo vs. 9 mo): $P = 0.0113$; n = 3/group; *SI Appendix*, Fig. S7*A*), and TSPO expression was significantly higher in APP-KI mice compared to WT mice at 9 mo of age (APP-KI 9 mo vs. WT 9 mo): $P = 0.0038$). Significantly increased TSPO immunoreactivity was observed in IBA-1$^+$ microglia clustered around and infiltrating Aβ plaques compared to microglia distal to plaques in both APP-KI mouse brain (*t* test: CI = −39.7, −19.8; $P = 0.0002$; n = 5/group; Fig. 4*F*) and human AD tissue (*t* test: CI = −21.6, −8.94; $P = 0.0016$; n = 7 AD brains; Fig. 4*G*).

TSPO Deletion Impairs Aβ Phagocytosis in Alzheimer's Mice and Exacerbates Pathology. Since our in vitro findings demonstrated that TSPO regulates phagocytosis and we observed increased TSPO expression in Aβ$^+$ microglial phagocytes in APP-KI mice, we examined whether TSPO knockdown affected the ability of these cells to phagocytose Aβ in APP-KI crossed with TSPO knockout mice (APP × TSPO-KO). APP × TSPO-KO mice exhibited a significant reduction in Aβ$^+$ phagocytic microglia compared to age-matched APP-KI mice (*t* test: CI = −7.77, −3.71; $P < 0.0001$; n = 5/group; Fig. 4*H*), despite no effect of TSPO-KO on total microglial numbers measured by flow cytometry or immunohistochemistry in APP-KI mice (all $P > 0.911$, Fig. 4 *H* and *I*). Reduced Aβ$^+$ phagocytic microglia numbers in APP × TSPO-KO mice was associated with increased amyloid load at 12 mo of age, compared to APP-KI mice (two-way ANOVA; Main Effect (Genotype): $F_{(1, 10)} = 8.094$ $P = 0.0174$; n = 3 to 4/group; Fig. 4*I*). No significant effect of TSPO-KO was observed on the percentage of lipid-droplet high microglia in APP mice (*t* test: CI = −1.82, 8.43; $P = 0.147$; n = 4 to 5/group; *SI Appendix*, Fig. S7*B*).

Mitochondrial HK Displacement Inhibits Glycolysis and Improves Phagocytic Function in TSPO-KO Microglia. We hypothesized that excessive mitochondrial HK recruitment in TSPO-KO microglia drove glycolysis, contributing to phagocytic impairment. To test this, we competitively displaced mitochondrial HK in TSPO-KO microglia using a cell-permeable, truncated N-terminal HK peptide fragment lacking the enzymatic domain (HKp, Fig. 5 *A*–*D*) (35). The ability of HKp to displace mitochondrial HK in microglia was verified by immunocytochemistry using BV2 cells (*t* test: CI = −82.1, −43.6, $P = 0.008$; n = 5; Fig. 5 *B* and *C*). HK displacement with HKp reduced glycolysis as measured by ECAR in TSPO-KO microglial cultures to WT levels (one-way ANOVA; $F_{(2, 23)} = 3.43$, $P = 0.049$; FDR corrected pairwise comparison scrambled peptide control in WT vs. TSPO-KO:

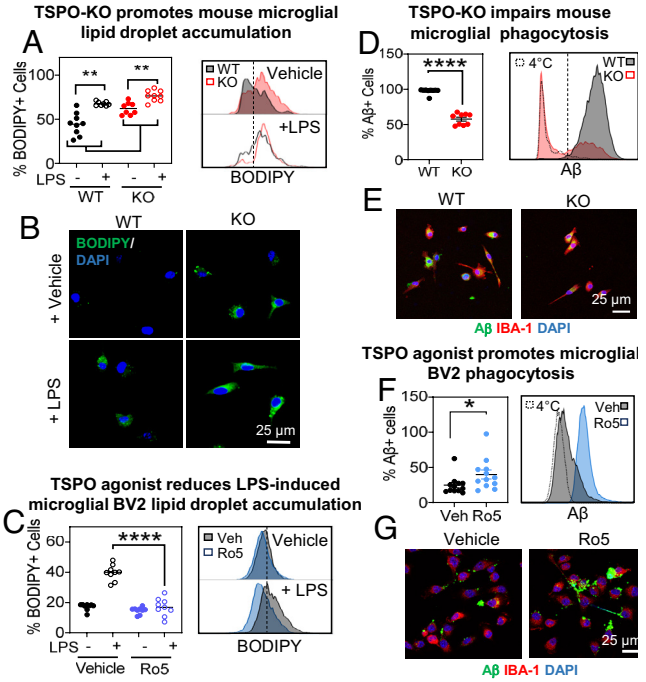

Fig. 3. TSPO deletion promotes lipid droplet accumulation and impairs phagocytosis in microglia. (*A*) Flow cytometry quantification (*Left*) and representative histogram (*Right*) of BODIPY+ cells in TSPO-KO and WT primary mouse microglia stimulated with or without LPS. Dots represent individual wells (n = 8 to 9/group, average of three experiments). (*B*) Representative confocal images of BODIPY (green) with DAPI (blue) staining in WT and TSPO-KO mouse microglial cultures. (*C*) Flow cytometry quantification (*Left*) and representative histogram (*Right*) of BODIPY^{+} cells in BV2 immortalized mouse microglia treated with TSPO agonist, Ro5-4864 (Ro5), or Vehicle. Dots represent individual wells (n = 9/group, average of three experiments). (*D* and *E*) Flow cytometry quantification (*D*) and representative confocal images of Aβ uptake (*E*) in TSPO-KO and WT cultured primary mouse microglia. Dots represent individual wells (n = 9/group, average of three experiments). Representative 4 °C control showing negligible surface binding of Aβ in absence of phagocytosis indicated on histoplot. (*F* and *G*) Flow cytometry quantification (*F*) and representative confocal images of Aβ uptake (*G*) in cultured BV2 microglia treated with TSPO agonist, Ro5-4864 (Ro5, 10 nM), or Vehicle (1% Ethanol). Dots represent individual wells (n = 12/group, average of three experiments). Representative 4 °C control showing negligible surface binding of Aβ in absence of phagocytosis indicated on histoplot. *A* and *C*: Two-way ANOVA including LPS and genotype (*A*) or treatment (*C*) as factors with Bonferroni-corrected pairwise comparisons. *D* and *F*: Unpaired two-sided permutation *t* test. **P* < 0.05, ***P* < 0.002, ****P* < 0.0001.

P = 0.03, TSPO-KO scrambled peptide vs. HKp: *P* = 0.03; n = 6 to 10 wells/treatment; Fig. 5*D*). These findings confirmed that the increase in glycolytic metabolism in TSPO-KO microglia was mediated by mitochondrial HK recruitment, which may be a compensatory response to the severe loss of mitochondrial ATP production.

Since hyperglycolysis is associated with impaired microglial function in aging and AD (2, 36–39), we hypothesized that excessive mitochondrial HK recruitment in the TSPO-KO microglia may contribute to their phagocytic dysfunction. To test this, we designed an optogenetic tool for light-activated recruitment of the HK-displacing peptide from the mitochondria to the PM, enabling reversible, spatial, and temporal control of mitochondrial HK. This was achieved by fusing a blue light-controlled dimerizing protein from the previously published improved light-induced dimer optogenetic system (40) to the C-terminal of HKp (HKp-sspb-RFP). This was coexpressed with the ssrA dimerization counterpart targeted to the PM using CAAX (ssrA-iLID-CAAX-venus) (Fig. 5*E*). In the absence of blue light, HKp localized to the mitochondria (mitochondria vs. PM *t* test: CI = −0.427, −0.208, *P* < 0.001; n = 5 cells/condition; Fig. 5*F*). With light activation, HKp was reversibly targeted to the PM (paired *t* test: preactivation vs. light-activated *t* = 3.61, *P* = 0.023; light-activated vs. reversal: *t* = 6.47, *P* = 0.003; Fig. 5 *G* and *H*). Light activation ('ON') increased glycolysis in microglial BV2 cells measured by ECAR in the Seahorse Glycostress test and lactate concentrations in the media (*t* test: ECAR, CI = −3.8, 18.6, *P* = 0.016, n = 12 wells average of two experiments; lactate, CI = −2.05, −1.16, *P* = 0.0004; n = 6 wells/group; Fig. 5 *I* and *J*). This provided us with a light-activated switch for the reversible control of subcellular HK localization in living cells.

We then used our optogenetic tool, which we have called GlycoSwitch, to test if HK displacement could rescue phagocytosis in cultured TSPO-KO microglia. HK displacement using GlycoSwitch increased phagocytosis by nearly 50% in TSPO-KO microglia (OFF vs. ON *t* test: CI = 5.57, 11.2, *P* < 0.0001; n = 4 wells/group, 1 outlier >2SD from mean excluded from statistical analysis, Fig. 5*K*). These findings indicate that excessive mitochondrial HK recruitment contributed to phagocytic dysfunction in TSPO-KO microglia.

Dynamic Regulation of Microglial Immunometabolism via Subcellular Localization of HK. Our findings indicate that in the absence of TSPO, HK is recruited to the mitochondria, driving glycolysis and contributing to phagocytic dysfunction. We then asked if mtHK binding/dissociation also plays a role in the coordination of normal microglial metabolic and immune responses to inflammatory stimuli. To test this, we expressed full-length HK-2 (FL-HK) or a truncated form of HK-2 (tHK) lacking the mitochondrial binding domain in BV2 microglia (Fig. 6*A*) (41). FL-HK localized predominantly to the mitochondria, while truncated HK localized to the cytosol (Fig. 6*A*). This enabled us to determine the relative significance of cytosolic vs. mitochondrial localization of HK to microglial metabolic and phagocytic function. First, we compared HK activity in BV2 cells expressing FL-HK vs. tHK, verifying that the HK enzymatic activity is regulated by mtHK binding. Reduced HK activity was observed in microglia expressing tHK, which cannot bind to the mitochondria (*t* test: CI = −4.46, −0.952, *P* = 0.036; Fig. 6*B*). This confirmed that mitochondrial HK localization regulates HK activity in microglia, an effect thought to be allosterically mediated upon binding to the TSPO complex member, VDAC (26).

We then compared the effect of FL-HK and tHK on glycolytic function under LPS-induced inflammatory conditions. To distinguish the functional significance of HK localization vs. HK enzymatic activity, we used a mutant form of HK (mHK) that binds to the mitochondria but is catalytically inactive (41). In LPS-stimulated microglial BV2 cells, the expression of FL-HK increased glycolysis compared to tHK and mHK (one-way ANOVA $F_{(4, 27)}$ = 8.49; *P* = 0.0002; FDR pairwise comparisons FL-HK vs. tHK *P* = 0.003, FL-HK vs. mHK *P* = 0.02; n = 6 to 8 wells/group; Fig. 6*C*). Reduced glycolysis in tHK and mHK expressing microglia was further corroborated by reduced lactate levels in the media (one-way ANOVA: $F_{(2, 14)}$ = 4.02, *P* = 0.046; FDR pairwise comparisons FL-HK vs. tHK *P* = 0.039, FL-HK vs. mHK *P* = 0.039; n = 5 wells/group; Fig. 6*D*). Similarly, mitochondrial displacement of HK with HKp reduced glycolytic capacity measured by ECAR in LPS stimulated primary mouse microglia, returning glycolysis to levels observed in unstimulated cells (one-way ANOVA: $F_{(2, 13)}$ = 9.882, *P* = 0.0025; LPS vs. LPS + HKp Bonferonni pairwise comparisons: *P* = 0.003; n = 5 to 6; Fig. 6*E*). No significant effect of HKp was observed on the mitochondrial membrane potential of BV2 microglia measured by TMRE fluorescence (*t*-test: CI = 4.47e+03, 6.08e+04; *P* = 0.076; n = 6/group,

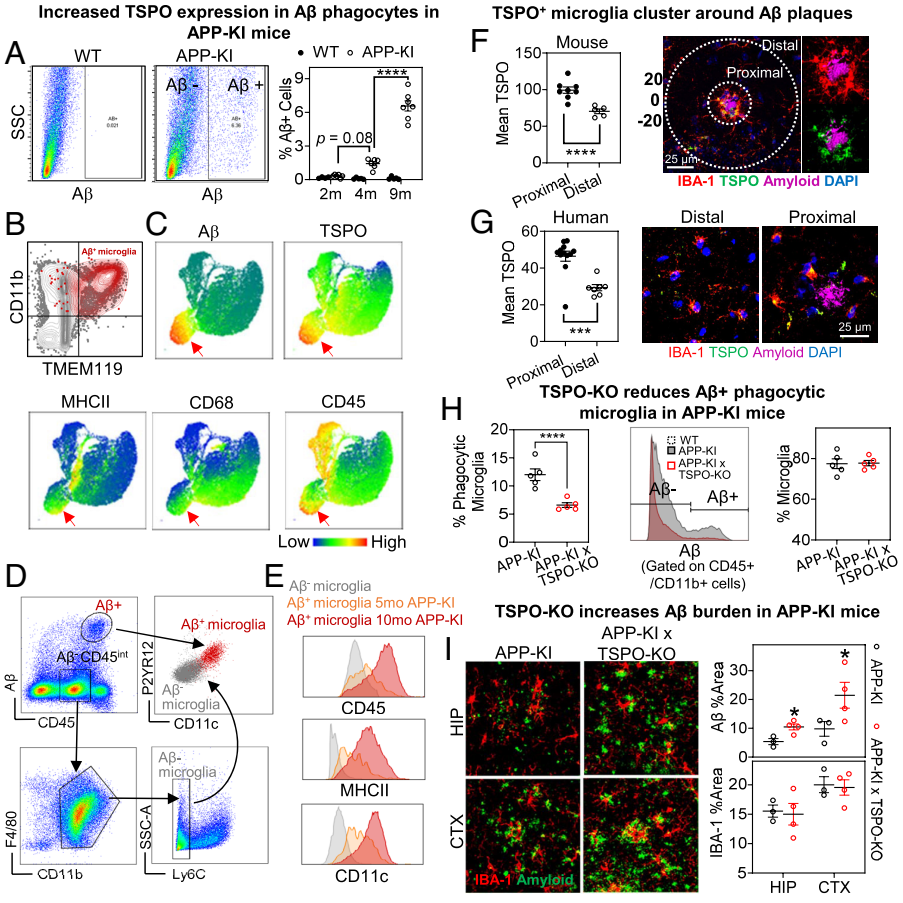

Fig. 4. TSPO deletion impairs Aβ phagocytosis in Alzheimer's mice and exacerbates pathology. (*A*) Representative flow cytometry gating of Aβ+ phagocytes in WT (*Left*) and APP-KI mice (*Middle*). Quantification of Aβ+ phagocytes in APP-KI mice at 2, 4, and 9 mo of age (*Right*, n = 6 to 7/group). Age-matched WT mice shown for comparison (n = 4 to 5/group). Dots in quantification graph represent individual brains. (*B*) Representative flow cytometry scatter plot showing CD11b and microglial marker, TMEM199 in Aβ+ cells isolated from APP-KI mouse (>9 mo age), confirming the $Aβ^+$ phagocytes are microglia. (*C*) Uniform manifold approximation and projection analysis showing 10,000 randomly sampled $CD45^+$ cells from 9-mo-old APP-KI mice (n = 7) with distribution of Aβ, TSPO, MHCII, CD68 and CD45 enriched populations indicated as a heatmap. Red arrow indicates $Aβ^+TSPO^{hi}$ population. (*D*) Representative flow cytometry histograms showing gating of $CD45^{hi}Aβ^+$ and $CD45^{int}Aβ^-$ microglial populations isolated from 10-mo-old APP-KI mouse and relative expression of CD11c and microglial marker P2RY12. (*E*) Flow cytometry histograms showing CD45, MHCII and CD11c increase with age/disease progression in $Aβ^+$ microglia (5 mo vs. 10 mo old APP-KI mice; concatenate of CD45+ cells, 5 mo group: n = 3 mice, 10 mo group: n = 5 mice). (*F* and *G*) Quantification and representative confocal images of TSPO immunoreactivity (TSPO-IR) in IBA-1+ microglia located proximal (10 μm) vs. distal (80 μm) to amyloid plaques in (*F*) APP-KI mice at 9 mo of age (n = 5/group) and (*G*) human AD brain (n = 7/group). (*H*) Flow cytometry quantification (*Left*) and representative histogram (*Middle*) of $Aβ^+$ microglial cells gated on $CD45^+/CD11b^+$ in 9-mo-old APP-KI and APP-KI × TSPO-KO mice. No difference in total isolated $CD45^+/CD11b^+$ microglia detected by flow cytometry (*Right*). Dots represent individual mouse brains (n = 5/group). (*I*) Quantification and representative confocal images of Aβ and IBA-1 immunoreactivity in 11-mo-old APP-KI and APP-KI × TSPO-KO mice (n = 3 to 4/group). HIP: hippocampus; CTX: cortex. A: One-way ANOVA analysis with Bonferroni pairwise comparisons used on APP-KI groups. *F*, *G*, and *H*: Unpaired two-sided permutational *t* test. *I*: Two-way ANOVA with Bonferonni corrected pairwise comparisons. ***$P < 0.001$, ****$P < 0.0001$.

average of two experiments; *SI Appendix*, Fig. S8*A*). Nor was any effect of FL-HK, tHK, or mHK expression observed on mitochondrial respiration in LPS-stimulated BV2 microglia as measured by OCR in the Seahorse Mitostress test (one-way ANOVA: $F_{(2, 15)} = 1.196$, $P = 0.33$; *SI Appendix*, Fig. S8*B*). These findings indicate that mtHK binding/dissociation is critical for coordination of microglial glycolytic reprogramming in response to LPS-induced inflammation.

Interestingly, we found that Aβ markedly increased mtHK binding in cultured primary mouse microglia (one-way ANOVA: $F_{(2, 117)} = 25.84$, $P < 0.0001$; Bonferonni pairwise comparisons Vehicle vs. Aβ $P < 0.0001$; n = 40/group, average of two experiments; Fig. 6 *F* and *G*). We hypothesized that Aβ may induce a switch to glycolytic metabolism in microglia in AD. Consistent with this, microglia isolated from APP-KI mice exhibit increased glycolysis and reduced mitochondrial respiration as measured by ECAR and OCR in the Seahorse, respectively (*t* test: glycolysis, CI = 8.85, 44.6, $P = 0.009$; maximal respiration CI = −98.6, −10.3, $P = 0.029$; ATP production CI = −1.02e+02, −4.24, $P = 0.053$; n = 9 to 11 mice/group; *SI Appendix*, Fig. S9). Since a switch from OXPHOS to glycolysis is associated with microglial phagocytic dysfunction in AD, we tested whether mtHK binding/dissociation regulated microglial phagocytic function. BV2 microglia expressing tHK exhibited higher phagocytic activity compared to cells expressing either FL-HK or mHK (one-way ANOVA: $F_{(2, 36)} = 11.78$, $P = 0.0001$; FDR pairwise comparisons tHK vs. FL-HK $P < 0.0001$, tHK vs. mHK $P = 0.0002$; n = 13 wells/group, average of three experiments; Fig. 6*H*). Given mutant HK did not induce phagocytosis compared to FL-HK, this suggested cytosolic HK may promote phagocytosis by a mechanism independent of its metabolic function. Supporting this, in contrast to tHK, inhibition of glycolysis with the nonmetabolizable analog glucose, 2-deoxyglucose (2-DG), inhibited phagocytosis (*t* test: CI = −10.95 to −2.249, $P = 0.013$; n = 3 wells/group; Fig. 6*I*). HK displacement using our optogenetic tool GlycoSwitch also increased BV2 microglial phagocytosis by nearly 20% (*t* test: CI = −22.3, −8.43, $P = 0.0004$;

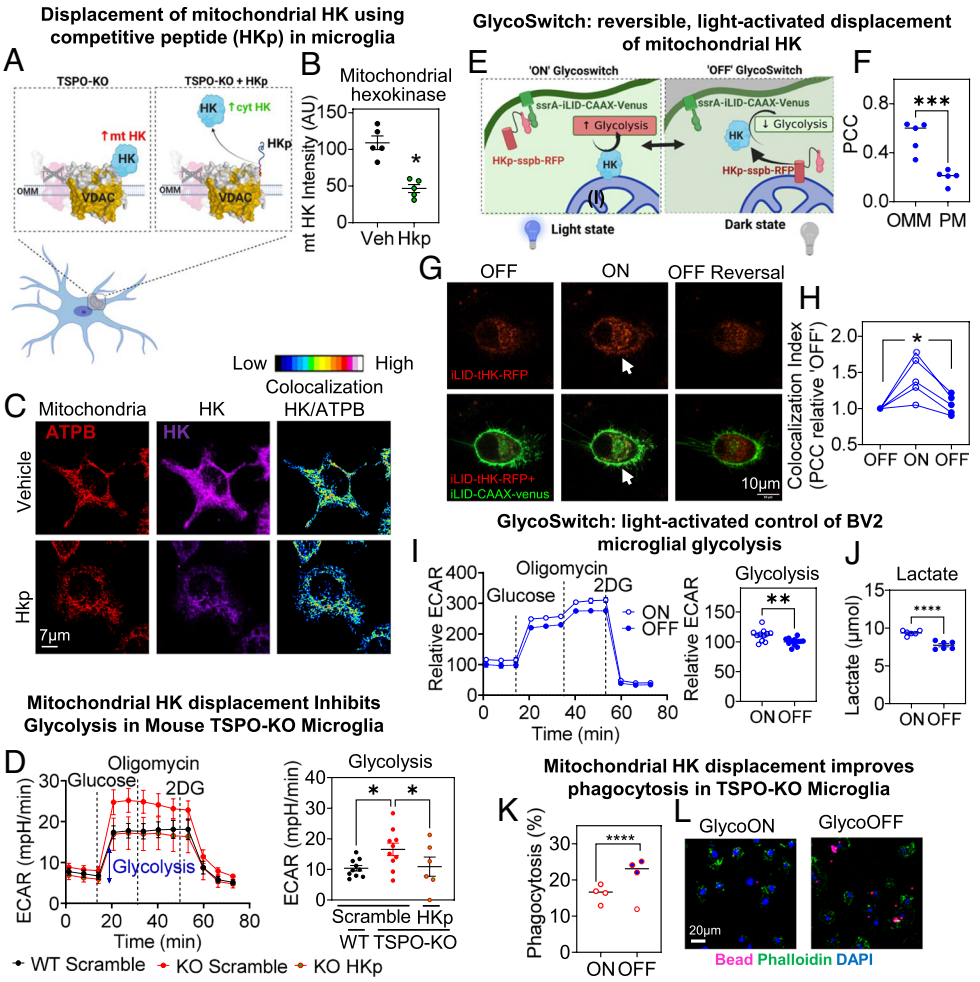

Fig. 5. Mitochondrial HK displacement inhibits glycolysis and improves phagocytosis in cultured TSPO-KO microglia. (*A*) Schematic showing strategy to competitively displace endogenous HK-2 (HK) from mitochondria using a cell permeable, truncated N-terminal HK peptide lacking the enzymatic domain (HKp). Created with BioRender.com. (*B*) Quantification of mtHK binding in BV2 microglia treated with vehicle or HKp. mtHK measured by mean HK immunoreactive intensity within mitochondrial volumes determined using immunostaining of mitochondrial marker, ATPB. Dots represent individual cells (n = 5/group). (*C*) Representative confocal images showing mitochondria (*Left*, ATPB, red), HK immunoreactivity (*Middle*, HK, purple) and colocalization index of HK relative to ATPB immunoreactivity (*Right*) in BV2 microglia following treatment with vehicle or HKp. (*D*) Glycolysis test curve (*Left*) and quantification of glycolysis (*Right*) in WT vs. TSPO-KO cultured microglia treated with either scrambled peptide (control) or HKp. Data shown as mean ± SEM ECAR. Dots represent individual wells (n = 6 wells/group). (*E*) Schematic of light-activated control of HKp-sspb-RFP localization. With light activation ("ON"), HKp-sspb-RFP translocates to the plasma membrane (PM) to bind ssrA-iLID-CAAX-Venus, enabling endogenous HK binding to the mitochondria and increasing glycolysis. In dark start ('OFF') HKp-sspb-RFP binds to the mitochondria, displacing endogenous mitochondrial HK and inhibiting glycolysis. (*F*) Colocalization index (Pearson correlation coefficient, PCC) of HKp-sspb-RFP with outer mitochondrial membrane vs. PM marker in dark state showing HKp localizes to mitochondria in OFF condition. (*G*) Representative live-cell confocal images of a cell expressing GlycoSwitch: HKp-sspb-RFP (red) coexpressed with ssrA-iLID-CAAX-Venus (green). Time-lapse of cell prior to blue-light stimulation (dark state, 'OFF"), following 1 min light-induced dimerization (light state, 'ON'), and following 2 min dark (dark state reversal, "OFF"). Arrow indicates region of co-localization after light stimulation. (*H*) Quantification of GlycoSwitch-HKp-RFP colocalization with the PM targeted dimer, GlycoSwitch-CAAX measured by PCC. Data normalized to prestimulation OFF condition. Individual dots represent single cells. (n = 5 cells). (*I*) Glycolysis test curve (*Left*) and quantification of glycolysis (*Right*) in BV2 cells expressing GlycoSwitch in either ON or OFF state. Data shown as mean ECAR ± SEM measured in the Seahorse Glycostress test. Data normalized to control group expressing optogenetic vector lacking the HKp domain. n = 12 wells/group, average of two experiments. (*J*) Lactate concentrations measured in media of BV2 microglia expressing GlycoSwitch in either ON or OFF state. Individual dots represent wells. n = 6/group. (*K*) Quantification of phagocytic uptake of latex beads measured by flow cytometry in cultured primary mouse TSPO-KO microglia expressing GlycoSwitch in either ON or OFF state. N = 4 well/group. Outlier indicated as hollow dot. (*L*) Representative confocal images of TSPO-KO microglia expressing GlycoSwitch activated in either OFF or ON state showing ingested beads (red), F-actin marker, phalloidin (green) and nuclear stain (DAPI, blue). *B* and *H–K*: Unpaired two-sided permutational *t* test. D: One-way ANOVA with FDR corrected pairwise comparisons. *F*: Paired two-sided *t* test. $^{*}P < 0.05$, $^{****}P < 0.0001$.

Fig. 6*J*). These findings suggest that disruption of mtHK binding may potentially be targeted to regulate microglial immunometabolic function and promote phagocytosis in Aβ-related neuropathology.

Discussion

Here, we provide insights into the mechanisms coordinating microglial metabolism to fuel phagocytosis, an important protective function in AD. We demonstrate that TSPO and HK play critical roles in the coordination of microglial respiratory-glycolytic metabolism and phagocytosis. TSPO was required for microglial energy production via OXPHOS to fuel phagocytosis. Microglia lacking TSPO resembled dysfunctional microglia observed in aging and AD. In the absence of TSPO, HK was recruited to the mitochondria, inducing glycolysis and contributing to phagocytic dysfunction. Aβ similarly induced excessive recruitment of HK to the mitochondria. Based on these findings, we propose that mitochondrial TSPO and HK together are a key mitochondrial hub regulating glycolytic-respiratory balance and phagocytosis of microglia and are promising targets for the development of novel immunotherapeutics in AD.

TSPO has been widely investigated as a biomarker of neuroinflammation in AD, and TSPO ligands exert protective effects by reducing Aβ accumulation in AD mouse models (5, 10). However, although commonly cited as a marker of 'detrimental inflammation', the precise immunophenotype associated with TSPO expression and how TSPO exerts its antiamyloidogenic effects are unknown. We provide evidence that TSPO plays a crucial role in promoting phagocytic clearance of Aβ via regulation of metabolic programming. In AD brains, TSPO-positive microglia clustered around Aβ plaques, and phagocytic microglia in AD mouse models were TSPO-enriched. This is consistent with previous studies showing enriched TSPO expression in microglia around plaques. For example, increased TSPO mRNA expression measured by single-cell RNAseq has been identified as a marker of the phagocytic 'disease-associated microglia' or DAMs (2, 42), and TSPO mRNA (34) and protein (2) were increased in Aβ+ phagocytic microglia isolated from the brains of AD mice. Further, we show that these TSPO-enriched

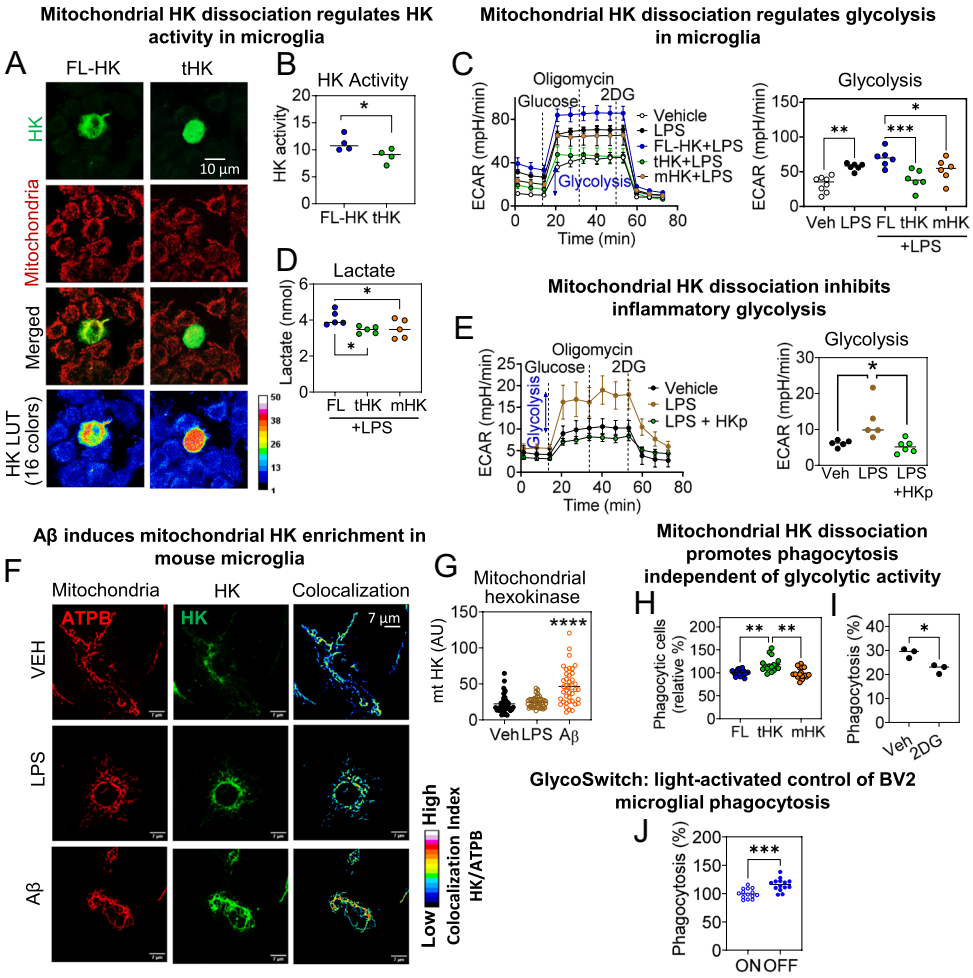

Fig. 6. mtHK binding/displacement regulates microglial glycolysis and phagocytic function in inflammation. (*A*) Representative confocal images of BV2 microglia expressing full-length HK (FL-HK, green, *Top* panel) and truncated HK (tHK, green, *Bottom* panel) after 1 h treatment with 500 nM Aβ. Mitochondrial (ATPB) costaining indicated in red. (*B*) HK activity measured in lysates of microglial BV2 cells expressing full length HK-2 (FL-HK) or truncated HK (tHK). Dots represent individual wells, n = 4/group. (*C*) Glycolysis test curve (*Left*) and quantification of glycolysis (*Right*) in vehicle (Veh) or LPS treated BV2 cells expressing FL-HK, tHK or mutant HK (mHK) measured in the Seahorse Glycostress test. Control vehicle and LPS groups were transfected with an empty vector control. Data shown as mean ± SEM ECAR. n = 6 wells/group. (*D*) Lactate concentrations measured in culture media of BV2 cells expressing FL-HK (FL), tHK or mHK. Dots represent individual wells. n = 5/group. (*E*) Glycolysis test curve (*Left*) and quantification of glycolysis (*Right*) in primary WT mouse microglia treated with either vehicle or LPS ± HKp showing mean ECAR ± SEM. n = 5 to 6 wells/group. (*F*) Representative confocal images showing mitochondria (*Left*, ATPB, red), HK immunoreactivity (*Middle*, HK, green) and colocalization index of HK relative to ATPB immunoreactivity (*Right*) in primary mouse microglia treated with vehicle (*Top*), LPS (*Middle*) or Aβ (*Bottom*). (*G*) Quantification of mitochondrial HK (mt HK) enrichment in cultured mouse microglia treated with vehicle, LPS or Aβ. Dots represent individual cells (n = 20/group). (*H*) Phagocytosis calculated as % cells ingested latex beads measured via flow cytometry in BV2 microglia expressing FL-HK (FL), tHK or mHK. Data expressed relative to FL-HK group. Dots represent individual wells. n = 16/group, average of four independent experiments. (*I*) Effect of 2DG compared to vehicle (Veh) on phagocytosis of latex beads in cultured microglial BV2 cells measured by flow cytometry. n = 3/group. (*J*) Quantification of phagocytic uptake of latex beads measured by flow cytometry in cultured immortalized microglial BV2 cells expressing GlycoSwitch activated in either ON or OFF state. Data expressed relative to ON group. Dots represent individual wells. n = 14 well/group, average of two independent experiments. *B*, *I*, and *J*: Unpaired two-sided permutational *t* test. *C–F* and *H*: One-way ANOVA with FDR pairwise comparisons. *$P < 0.05$, **$P < 0.003$, ***$P < 0.0002$.

prodromal AD have been associated with slower disease progression, consistent with a protective role of TSPO-associated inflammatory responses (44).

Interestingly, TSPO deletion induced a microglial phenotype that overlapped with dysfunctional microglia observed in aging, characterized by metabolic changes, accumulation of lipid droplets, and phagocytic impairment (31). For instance, Marschallinger et al. (31) identified a unique subpopulation of phagocytic-impaired microglia that exhibit increased lipid-droplet formation and increase with aging and AD. Lipids can be synthesized from acyl-CoA generated from metabolism of carbohydrates such as glucose. In aging and disease, this is linked to metabolic reprogramming from OXPHOS to glycolysis (30). We propose that TSPO deletion similarly results in a switch to conversion of glucose into lipids for storage. Supporting this, in the TSPO-KO mouse brain, transcriptional downregulation of genes involved in mitochondrial respiration and OXPHOS and upregulation of genes associated with lipid synthesis were observed. This included *ACLY*, a key enzyme involved in the shift from carbohydrate metabolism via the TCA cycle to cholesterol and fatty acid synthesis. This is consistent with previous studies that have reported altered OXPHOS following stimulation with TSPO ligands (45) or TSPO deletion (13) and additionally suggest that TSPO may affect lipid synthesis pathways to alter lipid droplet accumulation in microglia. TSPO has long been known to affect lipid biosynthesis and usage, specifically cholesterol, in other cell types, with a hypothesized role in steroidogenesis its most widely studied function. While recent genetic loss of function studies have shown that TSPO is not critical for steroidogenesis in the periphery (46, 47), TSPO deletion drastically reduced steroidogenesis in the brain (48). Although microglia are not steroidogenic cells, our findings suggest that TSPO may play a role in regulation of the synthesis of lipids including cholesterol from carbohydrates. Therefore, our findings may offer a potential alternative explanation of the effect of TSPO on steroidogenesis via effects on lipid synthesis from carbohydrate substrates to alter cholesterol bioavailability for steroidogenesis.

Microglial TSPO function was regulated by ligand binding. We demonstrated specific functional activation of TSPO via synthetic ligand binding to induce phagocytosis. Two key endogenous TSPO ligands, cholesterol and diazepine binding inhibitor (49),

microglia are characterized by high expression of several markers previously associated with phagocytic microglial phenotypes. This included CD11c, MHCII, and CD68. $CD11c^{+}$ microglial subpopulations have been described across a number of studies in AD and aging (see ref. 32 for full review), and these populations are characterized by enhanced capacity for uptake and lysosomal degradation of Aβ (43). These findings indicate that in AD, TSPO-PET signals are a marker of activated phagocytic microglia and therefore may be useful for monitoring the efficacy of novel immunotherapeutics aimed at promoting phagocytic function. Supporting this, elevated TSPO-PET signals in

are disrupted in microglia in AD. How these ligands affect microglial TSPO activity would be of high interest for future investigations. Structural changes in response to TSPO-ligand binding are thought to affect its stability (50), self-oligomerization (51, 52), or complex formation (e.g., ref. 53). Proteomic analysis of the TSPO interactome network identified the 14-3-3 family scaffold adaptor and chaperone proteins, as a hub in the TSPO-interactome network. The 14-3-3 adaptor proteins are metabolic regulators (54) and have been previously shown to interact with the TSPO complex in Leydig cells (55), with 14-3-3 adaptor phosphoserine protein binding motifs identified on functionally important sites on both TSPO and VDAC (55, 56). Our findings indicate these adaptor proteins may also be key components of the functional TSPO complex in the brain; future studies are needed to determine if these interactions are regulated by endogenous and synthetic ligands. Other previously reported interactors of the TSPO–VDAC complex identified here in the brain TSPO interactome included ATP synthase (Atp5a1) (57), mitochondrial solute carrier family 25 (58), and mitochondrial creatine kinase (59, 60). Interestingly, ATP synthase has also been previously shown to be regulated by the 14-3-3 adaptor proteins. TSPO interactions with the 14-3-3 adaptor proteins and ATP synthase may potentially explain how TSPO promotes OXPHOS. Since TSPO is predominantly expressed in microglia in the AD brain, TSPO-targeted drugs may provide a microglia-specific target to stimulate OXPHOS. This is of significance since, unlike TSPO-targeted drugs, most metabolic regulators either lack cell-type specificity or are toxic.

Unexpectedly, we found that elevated glycolysis in TSPO-KO microglia was mediated by a compensatory increase in activity of the glucose-metabolizing enzyme, HK. This was mediated by the recruitment of HK to the mitochondria. Previous studies have shown that HK binds to mitochondria through interaction with VDAC (26), which forms a complex with TSPO (58). In other cell types, mitochondrial HK recruitment is controlled by phosphorylation of either HK (61) or VDAC (62, 63). HK and VDAC are phosphorylated by protein kinase B (AKT) and the mechanistic target of rapamycin (mTOR) (62, 64), which are known key regulators of glycolysis in activated microglia (65). While the role of AKT and mTOR in HK mitochondrial recruitment remains to be verified in microglia, a previous study has shown altered VDAC phosphorylation levels in the AD brain (66) providing an avenue for investigation in the disease context. Furthermore, TSPO has also been shown to regulate VDAC phosphorylation (53), providing a potential avenue for crosstalk between TSPO and HK activity.

Mitochondrial HK displacement could at least in part rescue phagocytic defects in TSPO-KO microglia. A recent study has shown that inhibition of HK increases mitochondrial ATP production by inducing fatty acid oxidation (67). This may explain how mitochondrial HK displacement could rescue phagocytic deficits in TSPO-KO microglia despite severely impaired OXPHOS of glucose substrates. Interestingly, we found that cytosolic HK increased microglial phagocytosis independent of its enzymatic activity. This suggests that HK acts not only as a metabolic enzyme but also as an immune signaling molecule in microglia—integrating metabolic and immune responses. A previous study has similarly reported an immune signaling function of cytosolic HK in macrophages, where cytosolic HK signaled the activation of the NLRP3 inflammasome (35). These findings have two important implications. First, HK expression levels do not accurately reflect HK activity or function since changes in subcellular localization play an important role in the regulation of HK function. This has important conceptual implication for our understanding of mechanisms beyond transcriptional control in the regulation of microglial immunometabolism. Second, displacement of mitochondrial HK may provide an improved approach for regulation of microglial immunometabolic function compared to approaches aimed at inhibition of HK levels or activity. This is an important consideration in the development of potential therapeutics development targeting HK.

Materials and Methods

Detailed descriptions of methods are provided in the *SI Appendix*.

Animals and Treatments. C57BL/6 (WT), homozygous TSPO-KO (47), APP NL-G-F knock-in (APP-KI) (68), and APP-KI × TSPO-KO mice were used. All experiments were carried out in accordance with the National Advisory Committee for Laboratory Animal Research guidelines and approved by the by the NTU Institutional Animal Care and Use Committee (IACUC# A0384).

RNAseq Data Generation and Analysis. Total RNA was extracted from WT and TSPO-KO mouse hippocampus from animals treated with phosphate-buffered saline or LPS (from *Escherichia coli*, Sigma Aldrich; 1 mg/kg/day i.p. for 4 d). OligodT mRNAseq stranded library was prepared using NEBNext Ultra library preparation kit and sequenced using Illumina HiSeqTM. Differential expression analysis was performed using DESEQ2 (69). For gene set enrichment, fGSEA package (70) was used.

Immunoprecipitation Mass-Spectrometry (IP-MS). Proteins were IP from mouse brain homogenate using rabbit anti-TSPO antibody (Abcam 109497) and identified by LC-MS/MS. Differential enrichment analysis using Bioconductor R package Limma version 3.13 was used to identify candidate interactors (FDR < 10%, fold change > 2) (71). Network and functional enrichment analysis of identified candidate interactors was carried out using Cytoscape (72), InTact (73), and StringApp plugins version 3.8 (74).

Cell Culture and Treatments. Immortalized murine microglial BV2 cells (Accegen Biotechnology, ABC-TC212S) and primary microglia were derived from WT (C57BL/6J), and TSPO-KO neonatal mice (75) were used. Cells were transfected using lipofectamine 2000, and the following plasmids were purchased from Addgene: pLL7.0: ssrA-iLID-CAAX-venus (from KRas4.B) (Addgene #60411; deposited as a gift from Brian Kuhlman) (76), FLHKII-pGFPN3 (Addgene #21920), TrHKII-pGFPN3 (Addgene #21921), and MuHKII-pGFPN3 (Addgene #21922; deposited as a gift from Hossein Ardehali) (41). For light activation in the optogenetic studies, cells were illuminated with 500 $\mu W/cm^2$ white light irradiance from a LED for 1 h.

Mitochondrial Bioenergetics. OCR and ECAR were measured using an XFe96 Extracellular Flux Analyzer with the XF Cell Mito Stress Test Kit (#103015-100, Mitochondrial Biosciences) and Glycolysis Stress Test Kit (#103017-100). Lactate concentrations were measured using an L-Lactate Colorimetric Assay kit (ab65331, Abcam Plc, UK), and HK activity was measured using Hexokinase Activity Assay Kit (Abcam, ab136957).

In Vitro Phagocytosis Assay. Cultured BV2 cells or primary microglia were incubated with latex beads (Sigma Aldrich, L4530) or 500 nM fluorescently labeled oligomeric Aβ for 2 h. Uptake was measured by flow cytometry. To determine Aβ binding to the cell surface without phagocytic internalization, cells were incubated with Aβ at 4 °C.

Flow Cytometry. Myeloid cells were isolated from hemibrains as previously described (77) and incubated with anti-mouse CD16/32 followed by labeling with conjugated antibodies or dye. The following were used: CD11c (BD Horizon, clone: N418), CD11b (BioLegend,clone: M1/70), CD45 (BioLegend, clone: 30F11), F4/80 (BioLegend,clone: BM8), CD16/32 (BioLegend,clone: 93), MHCII (BioLegend,clone: M5/114.15.2), CD11c (BioLegend, clone: HL3), CD68 (BD Pharmigen, clone: FA/11), P2RY12 (BioLegend, 848006), TMEM119 (Ab225494, clone: 106-6), BODIPY–FLC12 (D3822, Thermo Fisher), and propidium iodide (P3566 Thermo Fisher). Cell suspensions were analyzed using an LSRII flow

cytometer (Becton Dickinson), and data were analyzed with FlowJo software (TreeStar).

Immunostaining. Fixed cells, mouse brain sections or post-mortem human brain sections were permeabilized with 0.1% Triton X-100 then immunostained before mounting in fluoroshield with DAPI (Abcam, ab104139). Primary antibodies used were rabbit anti-hexokinase (1:500, Abcam, ab227198), mouse anti-ATPB (1:1,000, Abcam, ab14730), rabbit anti-IBA-1 (1:500, Wako, 019-19741), rabbit anti-GFAP (Abcam, ab7260), Alexa Fluor 488 conjugated anti-PBR (Abcam, ab199779), and mouse anti-Aβ (Merck, MABN639). Phalloidin-647 (Abcam, ab176759) was used for F-actin labeling. Images were captured using a confocal microscope (Zeiss Laser Scanning Microscope-780 upright microscope) and analyzed using Imaris 9.2.0 or Image J/Fiji (78).

Statistical Analysis. GraphPad Prism 8.2.1 (GraphPad Software) or the online server at http://www.estimationstats.com (79) was used for statistical analyses and generation of plots.

Data, Materials, and Software Availability. Study data can be accessed via https://researchdata.ntu.edu.sg/dataverse/neurobiologyaging (80) and analysis pipelines are available at this link https://github.com/Neurobiology-Aging-and-Disease-Lab/Fairley-Lai-et-al- (81).

ACKNOWLEDGMENTS. We are grateful to Drs. Makoto Higuchi and Bin Ji (National Institutes for Quantum and Radiological Science and Technology, Japan) for the TSPO-KO mouse model; Drs. Takaomi Saido (RIKEN Center for Brain Science) and Takashi Saito (Nagoya City University Graduate School of Medical Sciences) for the APP-KI mouse model; Dr. Jianpeng Sheng (SBS, NTU) for technical assistance; School of Biological Sciences Mass Spectrometry Core Facility in Nanyang Technological University, Singapore for performing the Mass Spectrometry; UK Multiple Sclerosis and Parkinson's Tissue Bank at Imperial College London for the gift of post-mortem AD tissues; and Dr. Suresh Jesuthasan and his lab for assistance with cloning the GlycoSwitch construct and helpful comments on the manuscript. This project was funded by the Nanyang Assistant Professorship Award from Nanyang Technological University Singapore (A.M.B.) and the Ministry of Education, Singapore, under its Academic Research Fund Tier 1 (Project ID RG23/21; A.M.B.).

Author affiliations: [a]Neurobiology of Aging and Disease Laboratory, Lee Kong Chian School of Medicine, Nanyang Technological University Singapore, 308232, Singapore; [b]Lee Kong Chian School of Medicine, Nanyang Technological University Singapore, 308232, Singapore; [c]School of Biological Sciences, Nanyang Technological University Singapore, 637551, Singapore; and [d]Center for Molecular Neuropathology, Lee Kong Chian School of Medicine, Nanyang Technological University Singapore, 308232, Singapore

1. L. H. Fairley, J. H. Wong, A. M. Barron, Mitochondrial regulation of microglial immunometabolism in Alzheimer's disease. *Front. Immunol.* **12**, 624538 (2021).
2. E. C. B. Johnson *et al.*, Large-scale proteomic analysis of Alzheimer's disease brain and cerebrospinal fluid reveals early changes in energy metabolism associated with microglia and astrocyte activation. *Nat. Med.* **26**, 769–780 (2020).
3. C. Y. D. Lee, G. E. Landreth, The role of microglia in amyloid clearance from the AD brain. *J. Neural. Transm.* **117**, 949–960 (2010).
4. L. Zhang *et al.*, Recent developments on PET radiotracers for TSPO and their applications in neuroimaging. *Acta Pharm. Sin. B* **11**, 373–393 (2021).
5. A. M. Barron *et al.*, Ligand for translocator protein reverses pathology in a mouse model of Alzheimer's disease. *J. Neurosci.* **33**, 8891–8897 (2013).
6. R. Rupprecht *et al.*, Translocator protein (18 kDa) (TSPO) as a therapeutic target for neurological and psychiatric disorders. *Nat. Rev. Drug Discov.* **9**, 971–988 (2010).
7. L. H. Fairley *et al.*, Neuroprotective effect of mitochondrial translocator protein ligand in a mouse model of tauopathy. *J. Neuroinflammation* **18**, 76 (2021).
8. M. Dani *et al.*, Microglial activation correlates in vivo with both tau and amyloid in Alzheimer's disease. *Brain* **141**, 2740–2754 (2018).
9. W. C. Kreisl *et al.*, In vivo radioligand binding to translocator protein correlates with severity of Alzheimer's disease. *Brain* **136**, 2228–2238 (2013).
10. A. Christensen, C. J. Pike, TSPO ligand PK11195 improves Alzheimer-related outcomes in aged female 3xTg-AD mice. *Neurosci. Lett.* **683**, 7–12 (2018).
11. J. Choi, M. Ifuku, M. Noda, T. R. Guilarte, Translocator protein (18 kDa)/peripheral benzodiazepine receptor specific ligands induce microglia functions consistent with an activated state. *Glia* **59**, 219–230 (2011).
12. M. Karlstetter *et al.*, Translocator protein (18 kDa) (TSPO) is expressed in reactive retinal microglia and modulates microglial inflammation and phagocytosis. *J. Neuroinflammation* **11**, 3 (2014).
13. R. Yao *et al.*, Translocator protein 18 kDa (TSPO) deficiency inhibits microglial activation and impairs mitochondrial function. *Front Pharmacol.* **11**, 986 (2020).
14. R. B. Banati *et al.*, Positron emission tomography and functional characterization of a complete PBR/TSPO knockout. *Nat. Commun.* **5**, 5452 (2014).
15. Y. Fu *et al.*, TSPO deficiency induces mitochondrial dysfunction, leading to hypoxia, angiogenesis, and a growth-promoting metabolic shift toward glycolysis in glioblastoma. *Neuro Oncol.* **22**, 240–252 (2019).
16. V. M. Milenkovic *et al.*, CRISPR-Cas9 mediated TSPO gene knockout alters respiration and cellular metabolism in human primary microglia cells. *Int. J. Mol. Sci.* **20**, 3359 (2019).
17. S. Bader *et al.*, Differential effects of TSPO ligands on mitochondrial function in mouse microglia cells. *Psychoneuroendocrinol* **106**, 65–76 (2019).
18. S. H. Baik *et al.*, A breakdown in metabolic reprogramming causes microglia dysfunction in Alzheimer's disease. *Cell Metab.* **30**, 493–507.e6 (2019).
19. R. Holland *et al.*, Inflammatory microglia are glycolytic and iron retentive and typify the microglia in APP/PS1 mice. *Brain Behav. Immun.* **68**, 183–196 (2018).
20. S. Nair *et al.*, Lipopolysaccharide-induced alteration of mitochondrial morphology induces a metabolic shift in microglia modulating the inflammatory response in vitro and in vivo. *Glia* **67**, 1047–1061 (2019).
21. L. A. Voloboueva, J. F. Emery, X. Sun, R. G. Giffard, Inflammatory response of microglial BV-2 cells includes a glycolytic shift and is modulated by mitochondrial glucose-regulated protein 75/mortalin. *FEBS Lett.* **587**, 756–762 (2013).
22. Y. Wang *et al.*, TREM2-mediated early microglial response limits diffusion and toxicity of amyloid plaques. *J. Exp. Med.* **213**, 667–675 (2016).
23. E. N. Maldonado *et al.*, Voltage-dependent anion channels modulate mitochondrial metabolism in cancer cells: Regulation by free tubulin and erastin. *J. Biol. Chem.* **288**, 11920–11929 (2013).
24. K. K. Arora, P. L. Pedersen, Functional significance of mitochondrial bound hexokinase in tumor cell metabolism. Evidence for preferential phosphorylation of glucose by intramitochondrially generated ATP. *J. Biol. Chem.* **263**, 17422–17428 (1988).
25. J. J. Lemasters, E. Holmuhamedov, Voltage-dependent anion channel (VDAC) as mitochondrial governator–thinking outside the box. *Biochim. Biophys Acta* **1762**, 181–190 (2006).
26. D. J. Roberts, S. Miyamoto, Hexokinase II integrates energy metabolism and cellular protection: Akting on mitochondria and TORCing to autophagy. *Cell Death Differ.* **22**, 248–257 (2015).
27. Y. Li *et al.*, Hexokinase 2-dependent hyperglycolysis driving microglial activation contributes to ischemic brain injury. *J. Neurochem.* **144**, 186–200 (2018).
28. K. Sharma *et al.*, Cell type– and brain region–resolved mouse brain proteome. *Nat. Neurosci.* **18**, 1819–1831 (2015).
29. M. Colombini, VDAC: The channel at the interface between mitochondria and the cytosol. *Mol. Cell Biochem.* **256**, 107–115 (2004).
30. J. Fussell *et al.*, 166-A lipogenic-switch shifts metabolism from glycolysis to mitochondrial respiration during aging. *Free Rad. Biol. Med.* **100**, S83 (2016).
31. J. Marschallinger *et al.*, Lipid-droplet-accumulating microglia represent a dysfunctional and proinflammatory state in the aging brain. *Nat. Neurosci.* **23**, 194–208 (2020).
32. A. Benmamar-Badel, T. Owens, A. Wlodarczyk, Protective microglial subset in development, aging, and disease: Lessons from transcriptomic studies. *Front. Immunol.* **11**, 430 (2020).
33. S. Rangaraju *et al.*, Differential phagocytic properties of CD45(low) microglia and CD45(high) brain mononuclear phagocytes-activation and age-related effects. *Front. Immunol.* **9**, 405 (2018).
34. A. Grubman *et al.*, Transcriptional signature in microglia associated with Aβ plaque phagocytosis. *Nat. Commun.* **12**, 3015 (2021).
35. A. J. Wolf *et al.*, Hexokinase is an innate immune receptor for the detection of bacterial peptidoglycan. *Cell* **166**, 624–636 (2016).
36. A. McIntosh *et al.*, Iron accumulation in microglia triggers a cascade of events that leads to altered metabolism and compromised function in APP/PS1 mice. *Brain Pathol.* **29**, 606–621 (2019).
37. A. G. Vlassenko *et al.*, Spatial correlation between brain aerobic glycolysis and amyloid-β (Aβ) deposition. *Proc. Natl. Acad. Sci. U.S.A.* **107**, 17763–17767 (2010).
38. L. Sebastian Monasor *et al.*, Fibrillar Aβ triggers microglial proteome alterations and dysfunction in Alzheimer mouse models. *Elife* **9**, e54083 (2020).
39. A. Rubio-Araiz, O. M. Finucane, S. Keogh, M. A. Lynch, Anti-TLR2 antibody triggers oxidative phosphorylation in microglia and increases phagocytosis of β-amyloid. *J. Neuroinflamm.* **15**, 247 (2018).
40. G. Guntas *et al.*, Engineering an improved light-induced dimer (iLID) for controlling the localization and activity of signaling proteins. *Proc. Natl. Acad. Sci. U.S.A.* **112**, 112–117 (2015).
41. L. Sun, S. Shukair, T. J. Naik, F. Moazed, H. Ardehali, Glucose phosphorylation and mitochondrial binding are required for the protective effects of hexokinases I and II. *Mol. Cell Biol.* **28**, 1007–1017 (2008).
42. H. Keren-Shaul *et al.*, A unique microglia type associated with restricting development of Alzheimer's disease. *Cell* **169**, 1276–1290.e17 (2017).
43. W. Kamphuis, L. Kooijman, S. Schetters, M. Orre, E. M. Hol, Transcriptional profiling of CD11c-positive microglia accumulating around amyloid plaques in a mouse model for Alzheimer's disease. *Biochim. Biophys. Acta* **1862**, 1847–1860 (2016).
44. L. Hamelin *et al.*, Early and protective microglial activation in Alzheimer's disease: A prospective study using 18F-DPA-714 PET imaging. *Brain* **139**, 1252–1264 (2016).
45. I. Lejri *et al.*, TSPO ligands boost mitochondrial function and pregnenolone synthesis. *J. Alzheimers Dis.* **72**, 1045–1058 (2019), 10.3233/JAD-190127.
46. J. Fan, E. Campioli, A. Midzak, M. Culty, V. Papadopoulos, Conditional steroidogenic cell-targeted deletion of TSPO unveils a crucial role in viability and hormone-dependent steroid formation. *Proc. Natl. Acad. Sci. U.S.A.* **112**, 7261–7266 (2015).
47. A. M. Barron, B. Ji, S. Kito, T. Suhara, M. Higuchi, Steroidogenic abnormalities in translocator protein knockout mice and significance in the aging male. *Biochem. J.* **475**, BCJ20170645 (2017), 10.1042/bcj20170645.
48. A. M. Barron *et al.*, Regulation of anxiety and depression by mitochondrial translocator protein-mediated steroidogenesis: The role of neurons. *Mol. Neurobiol.* **58**, 550–563 (2021).
49. J. Jiang, C. Wang, R. Qi, H. Fu, Q. Ma, scREAD: A single-cell RNA-seq database for Alzheimer's disease. *iScience* **23**, 101769 (2020).
50. V. M. Milenkovic *et al.*, Effects of genetic variants in the TSPO gene on protein structure and stability. *PLoS One* **13**, e0195627 (2018).
51. L. Jaremko, M. Jaremko, S. Becker, M. Zweckstetter, Toward the functional oligomerization state of tryptophan-rich sensory proteins. *Protein Sci.* **23**, 1154–1160 (2014).

52. F. Li, Y. Xia, J. Meiler, S. Ferguson-Miller, Characterization and modeling of the oligomeric state and ligand binding behavior of purified translocator protein 18 kDa from Rhodobacter sphaeroides. *Biochemistry* **52**, 5884–5899 (2013).
53. J. Gatliff *et al.*, TSPO interacts with VDAC1 and triggers a ROS-mediated inhibition of mitochondrial quality control. *Autophagy* **10**, 2279–2296 (2014).
54. R. Kleppe, A. Martinez, S. O. Døskeland, J. Haavik, The 14-3-3 proteins in regulation of cellular metabolism. *Semin. Cell Dev. Biol.* **22**, 713–719 (2011).
55. Y. Aghazadeh, D. B. Martinez-Arguelles, J. Fan, M. Culty, V. Papadopoulos, Induction of androgen formation in the male by a TAT-VDAC1 fusion peptide blocking 14-3-3ε protein adaptor and mitochondrial VDAC1 interactions. *Mol. Ther.* **22**, 1779–1791 (2014).
56. Y. Aghazadeh *et al.*, Hormone-induced 14-3-3γ adaptor protein regulates steroidogenic acute regulatory protein activity and steroid biosynthesis in MA-10 Leydig cells. *J. Biol. Chem.* **287**, 15380–15394 (2012).
57. L. Veenman *et al.*, Potential involvement of F0F1-ATP(synth)ase and reactive oxygen species in apoptosis induction by the antineoplastic agent erucylphosphohomocholine in glioblastoma cell lines: A mechanism for induction of apoptosis via the 18 kDa mitochondrial translocator protein. *Apoptosis* **15**, 753–768 (2010).
58. M. W. McEnery, A. M. Snowman, R. R. Trifiletti, S. H. Snyder, Isolation of the mitochondrial benzodiazepine receptor: Association with the voltage-dependent anion channel and the adenine nucleotide carrier. *Proc. Natl. Acad. Sci. U.S.A.* **89**, 3170–3174 (1992).
59. G. Beutner, A. Ruck, B. Riede, W. Welte, D. Brdiczka, Complexes between kinases, mitochondrial porin and adenylate translocator in rat brain resemble the permeability transition pore. *FEBS Lett.* **396**, 189–195 (1996).
60. C. Datler *et al.*, CKMT1 regulates the mitochondrial permeability transition pore in a process that provides evidence for alternative forms of the complex. *J. Cell Sci.* **127**, 1816–1828 (2014).
61. S. Miyamoto, A. N. Murphy, J. H. Brown, Akt mediates mitochondrial protection in cardiomyocytes through phosphorylation of mitochondrial hexokinase-II. *Cell Death Differ.* **15**, 521–529 (2008).
62. J. G. Pastorino, J. B. Hoek, N. Shulga, Activation of glycogen synthase kinase 3beta disrupts the binding of hexokinase II to mitochondria by phosphorylating voltage-dependent anion channel and potentiates chemotherapy-induced cytotoxicity. *Cancer Res.* **65**, 10545–10554 (2005).
63. L. Galluzzi, O. Kepp, N. Tajeddine, G. Kroemer, Disruption of the hexokinase–VDAC complex for tumor therapy. *Oncogene* **27**, 4633–4635 (2008).
64. S. Das, R. Wong, N. Rajapakse, E. Murphy, C. Steenbergen, Glycogen synthase kinase 3 inhibition slows mitochondrial adenine nucleotide transport and regulates voltage-dependent anion channel phosphorylation. *Circ. Res.* **103**, 983–991 (2008).
65. S. Yang *et al.*, Microglia reprogram metabolic profiles for phenotype and function changes in central nervous system. *Neurobiol. Dis.* **152**, 105290 (2021).
66. M. Cuadrado-Tejedor *et al.*, Enhanced expression of the voltage-dependent anion channel 1 (VDAC1) in Alzheimer's disease transgenic mice: An insight into the pathogenic effects of amyloid-β. *J. Alzheimers Dis.* **23**, 195–206 (2011).
67. L. Leng *et al.*, Microglial hexokinase 2 deficiency increases ATP generation through lipid metabolism leading to β-amyloid clearance. *Nat. Metabol.* **4**, 1287–1305 (2022), 10.1038/s42255-022-00643-4.
68. T. Saito *et al.*, Single App knock-in mouse models of Alzheimer's disease. *Nat. Neurosci.* **17**, 661–663 (2014).
69. M. I. Love, W. Huber, S. Anders, Moderated estimation of fold change and dispersion for RNA-seq data with DESeq2. *Genome Biol.* **15**, 550 (2014).
70. G. Korotkevich *et al.*, Fast gene set enrichment analysis. bioRxiv [Preprint] (2021), https://doi.org/10.1101/060012 (Accessed 13 June 2020).
71. M. E. Ritchie *et al.*, limma powers differential expression analyses for RNA-sequencing and microarray studies. *Nucleic Acids Res.* **43**, e47 (2015).
72. P. Shannon *et al.*, Cytoscape: A software environment for integrated models of biomolecular interaction networks. *Genome Res.* **13**, 2498–2504 (2003).
73. H. Hermjakob *et al.*, IntAct: An open source molecular interaction database. *Nucleic Acids Res.* **32**, D452–D455 (2004).
74. N. T. Doncheva, J. H. Morris, J. Gorodkin, L. J. Jensen, Cytoscape stringApp: Network analysis and visualization of proteomics data. *J. Proteome Res.* **18**, 623–632 (2019).
75. H. Lian, E. Roy, H. Zheng, Protocol for primary microglial culture preparation. *Bio. Protoc.* **6**, e1989 (2016).
76. G. Guntas *et al.*, Engineering an improved light-induced dimer (iLID) for controlling the localization and activity of signaling proteins. *Proc. Natl. Acad. Sci. U.S.A.* **112**, 112–117 (2015).
77. J. Sheng, C. Ruedl, K. Karjalainen, Most tissue-resident macrophages except microglia are derived from fetal hematopoietic stem cells. *Immunity* **43**, 382–393 (2015).
78. J. Schindelin *et al.*, Fiji: An open-source platform for biological-image analysis. *Nat. Methods* **9**, 676–682 (2012).
79. J. Ho, T. Tumkaya, S. Aryal, H. Choi, A. Claridge-Chang, Moving beyond P values: Data analysis with estimation graphics. *Nat. Methods* **16**, 565–566 (2019).
80. K. O. Lai *et al.*, Mitochondrial control of microglial phagocytosis by the translocator protein and hexokinase 2 in Alzheimer's disease. *DR-NTU (Data)*. https://doi.org/10.21979/N9/TE6G9X. Deposited 31 Jan 2023.
81. K. O. Lai *et al.*, Neurobiology-Aging-and-Disease-Lab/Fairley-Lai-*et-al*-. *Github*. https://github.com/Neurobiology-Aging-and-Disease-Lab/Fairley-Lai-et-al-. Deposited 21 November 2021.